



Research article

One-day examination of triple nuclear medicine imaging and application in evaluating transarterial embolization

Nan Du^{a,b,c,1}, Guorong Jia^{d,1}, Wen Zhang^{a,b,c,1}, Qianqian Tong^d, Xudong Qu^{a,b,c}, Rong Liu^{a,b,c}, Danni Li^d, Zhiping Yan^{a,b,c}, Changjing Zuo^d, Xiao Li^{d,e,*}, Rou Li^{d,**}, Wei Zhang^{a,b,c,***}

^a Department of Interventional Radiology, Zhongshan Hospital, Fudan University, Shanghai, 200032, China

^b Shanghai Institution of Medical Imaging, Shanghai, 200032, China

^c National Clinical Research Center for Interventional Medicine, Shanghai, 200032, China

^d Department of Nuclear Medicine, Changhai Hospital, Naval Medical University, Shanghai, 200433, China

^e Shanghai Institute of Applied Physics, Chinese Academy of Sciences, Shanghai, 201800, China

ARTICLE INFO

Keywords:

Nuclear medicine imaging
Transarterial embolization
Tumor evaluation
One-day examination
Liver cancer
Neovascularization
Hypoxia
Tumor metabolism

ABSTRACT

A diagnosis based on multiple nuclear medicine imaging (NMI) was more comprehensive in approaching the nature of pathological changes. In this research, a method to realize triple NMIs within one day was developed based on the reasonable arrangements of ⁶⁸Ga-RGD PET/CT specialized on neovascularization, ^{99m}Tc-HL-91 SPECT/CT specialized on hypoxia and ¹⁸F-FDG PET/CT specialized on tumor metabolism. Feasibility was verified in evaluating the therapeutic effects of transarterial embolization (TAE) performed on rabbit models with VX2 tumor. Radiation dosimetry was carried out to record the radiation exposure from multiple injections of radiopharmaceuticals. In results, the one-day examination of triple NMIs manifested the diversity of the postoperative histological changes, including the local neovascularization induced by embolization, hypoxic state of embolized tissues, and suppression of tumor metabolism. More importantly, radiation dosage from radiopharmaceuticals was limited below 5.70 ± 0.90 mSv. In conclusion, the strong timeliness and complementarity of one-day examination of triple nuclear medicine imaging made it clinically operative and worthy of popularizing. There was flexibility in combining distinct NMIs according to the clinical demands, so as to provide comprehensive information for diagnosis.

* Corresponding author.

** Corresponding author.

*** Corresponding author. Department of Interventional Radiology, Zhongshan Hospital, Fudan University, Shanghai, 200032, China.

E-mail addresses: du.nan@zs-hospital.sh.cn (N. Du), jiagurong79@163.com (G. Jia), zhang.wen@zs-hospital.sh.cn (W. Zhang), tongqianqianzz@163.com (Q. Tong), qu.xudong@zs-hospital.sh.cn (X. Qu), liu.rong@zs-hospital.sh.cn (R. Liu), danny0524@sina.com (D. Li), yan.zhiping@zs-hospital.sh.cn (Z. Yan), changjing.zuo@qq.com (C. Zuo), lixiao_nm@smmu.edu.cn (X. Li), lr823049@163.com (R. Li), zhang.wei6@zs-hospital.sh.cn (W. Zhang).

¹ These three authors contributed equally to this work.

<https://doi.org/10.1016/j.heliyon.2024.e29597>

Received 22 August 2022; Received in revised form 8 April 2024; Accepted 10 April 2024

Available online 24 April 2024

2405-8440/© 2024 The Authors. Published by Elsevier Ltd. This is an open access article under the CC BY-NC license (<http://creativecommons.org/licenses/by-nc/4.0/>).

1. Introduction

Nuclear medicine imaging (NMI) has been widely used in clinic, because of the precise diagnosis of biochemical information. However, unlike the one-by-one usage of multiple sequences in one magnetic resonance imaging (MRI), the multiple uses of NMI were limited by the physical decay of medical nuclides. In most situations of one-day examination, only one scan can be applied on the basis of a single injection of radiopharmaceutical. Hence, the comprehensive diagnosis of tumors via multiple NMIs in a limited time was unpractical so far.

In the concrete, there were a lot of attempts to solve this issue. Firstly, a “cock-tail” protocol was developed on the basis of tracers’ differences on *in vivo* metabolism. For example, a method with co-injection of ^{18}F -FDG and $^{18}\text{F}^-$ ion has been used in the diagnosis of malignancy, such as sarcoma, breast cancer, colon cancer and lung cancer [1,2]. Post-processing of mixed signals from two tracers was necessarily performed on the basis of metabolic difference. Secondly, a method based on simultaneous injection of multiple gamma-emitters was developed for full energy spectrum scanning of SPECT. Separation of image data package relied on the distinctive peak values of tracers, such as $^{201}\text{Tl}/^{99\text{m}}\text{Tc}$ -MIBI in myocardial perfusion imaging, $^{201}\text{Tl}/^{99\text{m}}\text{Tc}$ -RBC in cardiac blood pool imaging and $^{201}\text{Tl}/^{123}\text{I}$ -BMIPP in myocardial ischemia [3–5], but the crossover of peak values and the diffraction from higher energy peak was inevitable, limiting the complexity in the arrangement of co-injected radiopharmaceuticals. Thirdly, those nuclides with short physical half-time, such as C-11, N-13, O-15, and so on, decayed soon (usually in minutes) to a natural radiation background before the subsequent NMI [6]. The short physical decay of nuclides together with the quick biological metabolism of tracers, such as H_2^{15}O , $^{13}\text{NH}_3$ and $^{82}\text{RbCl}$, built certain flexibility for one-day examination of multiple NMIs. Moreover, dual-tracer PET administration with ^{18}F -FDG and ^{68}Ga -FAPI-46 was demonstrated with the feasibility and potential in cancer imaging, and the dual-tracer approach may have superior sensitivity to ^{18}F -FDG PET alone without compromising individual assessment of either scan [7]. Therefore, the reasonable combination of radiopharmaceuticals and the artificial intelligent post-processing both contribute to the development of multiple NMI.

In clinic, how to shorten the diagnosis procedure is a crucial challenge to improving and accelerating the treatment of patients, especially for the accurate definition of neoplastic pathologies [8]. Combining two or more NMIs can effectively increase the specificity and sensitivity of diagnosing subtle pathological changes. For instance, diagnosing and localizing the prostate cancer (PCa) benefited from one or more of these below perspectives, ^{18}F -FDHT PET in evaluating androgen receptor expression in patients with advanced PCa, ^{18}F -FECH PET in diagnosing primary and metastatic lesions of PCa, ^{68}Ga -PSMA or ^{18}F -PSMA PET in evaluating PSMA expression and detecting tiny lesions and biochemical recurrence, and ^{18}F -FDG PET in evaluating tumor metabolism [9–11]. Notably, the combination does not mean the adoption of all-related examination, and the reasonable choice and arrangement accomplish more with less. For example, the combination of functional imaging for neuroendocrine tumors, including ^{18}F -FDG PET/CT and ^{68}Ga -DOTATATE PET/CT, is a well-described strategy for tumor staging and directs the management of patients with more confidence [12].

Realizing the one-day examination of multiple NMIs was meaningful for clinical diagnosis and social value. In this research, the stepwise scans of ^{68}Ga -RGD PET/CT, $^{99\text{m}}\text{Tc}$ -HL-91 SPECT/CT, and ^{18}F -FDG PET/CT were performed within 12 h, a routine period of one-day examination. The mutual interference of radiopharmaceuticals was assessed *in vitro*. The diagnostic value of triple NMIs was evaluated in VX2 tumor-bearing rabbits that were treated with transarterial embolization (TAE), which potentially led to neovascularization, hypoxia and tumor suppression in a short time [13–15].

2. Methods

2.1. Characterizations of mixed radiopharmaceuticals

^{18}F -FDG was purchased from Shanghai Atom Kexing Pharmaceuticals Co., Ltd. ^{68}Ga -RGD and $^{99\text{m}}\text{Tc}$ -HL-91 were prepared in-house according to the instructions of labeling kits (Shanghai Nice-labeling Biotechnology Co., Ltd). For the radiochemical stability evaluation of radiopharmaceutical in mixture with others, the saline-containing tracer was mixed with the corresponding precursor or analogue of the other two tracers of milligram grade, far greater than the chemical amount in radio-labeling. In detail, ^{18}F -FDG was mixed with DOTA-RGD and 4,9-diaza-3,3,10,10-tetramethyldecane-2,11-dione dioxime (HL-91); ^{68}Ga -RGD was mixed with glucose and HL-91; $^{99\text{m}}\text{Tc}$ -HL-91 was mixed with glucose and DOTA-RGD. The *in vivo* stability of radiopharmaceuticals was not evaluated due to the already-proved *in vivo* stability and the widely clinical use as a single tracer.

The *in vitro* stabilities of radiopharmaceuticals in the mixture were assessed in different systems, and the time points of evaluation were set in consideration of the time points of corresponding nuclear medicine imaging scans. For ^{18}F -FDG, the *in vitro* stability was measured at 0.5, 1 and 2 h after the mixing using thin layer chromatography with a radio-detector (radio-TLC) with 95 % acetonitrile in water as mobile phase and silica gel thin layer as solid phase. For ^{68}Ga -RGD, the *in vitro* stability was measured at 0.5 and 1 h after the mixing using radio-TLC with a mixture of 1 M $\text{NH}_4\text{OAc}/\text{CH}_3\text{OH}$ (1:1) as mobile phase and glass microfiber chromatography paper impregnated with silica gel (iTLC-SG) as solid phase. For $^{99\text{m}}\text{Tc}$ -HL-91, the *in vitro* stability was measured at 0.5, 1 and 2 h after the mixing using radio-TLC to detect free Tc-99 m as ions with acetone as mobile phase and iTLC-SG as solid phase, or to detect Tc-99m-based colloid with a mixture of 1 M $\text{NH}_4\text{OAc}/\text{CH}_3\text{OH}$ (1:1) as mobile phase and iTLC-SG as solid phase.

2.2. Preparation of tumor-bearing rabbit models and transarterial embolization

Adult New Zealand white rabbits (male, six months old, 2.2–2.5 kg) were used for this study. This research was approved by the Committee on Ethics of Medicine of Navy Medical University (No. 8220072600). The VX2 tumors were transplanted in the hind limb of

carrier rabbit. When the subcutaneous tumor reached about 0.8–1 cm in diameter, the tumorous tissue was harvested and cut into small cubes (approximately 1 mm³), and then implanted into the left lobe of a healthy liver. Three weeks after implantation, the liver tumors were considered in an ideal condition for embolization.

Embolization of the hepatic artery with lipiodol emulsion was performed in all three rabbit livers with the same procedures. TAE was performed under digital subtraction arteriography (DSA; AlluraXperFD20, Philips) and fluoroscopic guidance. The 2.8F micro-catheter (Boston Scientific) was introduced via the femoral artery and then advanced to super-select the left hepatic artery based on the angiography. The lipiodol was administered into the artery until the reflux of lipiodol emulsion under fluoroscopic was observed, and the injected dose of lipiodol was recorded. Typically, the average total usage of lipiodol was 0.8 mL.

2.3. Performance of one-day examination of triple nuclear medicine imaging

The multiple NMI examination was performed at 9 days post TAE. Fig. 1 provided the schematic diagram of the one-day examination of triple nuclear medicine imaging, including the tracer injection, dieting plan, scans schedule and narcotism. In consideration of the physical half-time of radio-nuclides and biological half-time of precursor, the scanning schedule was arranged as: firstly, ⁶⁸Ga-RGD PET/CT without fasting for solids and liquids; secondly, ^{99m}Tc-HL-91 SPECT/CT with a 9 h interval between the two injections, and the scan was performed at 1.5 h post injection (h P.I.); thirdly, ¹⁸F-FDG PET/CT immediately after the SPECT/CT scan, and the scan was performed at 45 min post injection (min P.I.). During the triple scans, rabbit models were kept abrosia, and provided with a normal diet after the completion of ¹⁸F-FDG PET/CT.

For ⁶⁸Ga-RGD PET/CT, after being anesthetized with isoflurane, 3.7 MBq ⁶⁸Ga-RGD per kilogram body weight were injected into the ear vein of tumor-bearing rabbits. PET/CT imaging was performed at 45 min P.I. using a clinical PET/CT scanner (Biograph64, Siemens, Germany). In a standard PET/CT scan for ⁶⁸Ga-RGD or ¹⁸F-FDG, a low-dose CT scan was followed by PET scan. Image acquisition parameters were set as follows: for CT, tube voltage: 120 kV; tube current: 35 mA; pitch: 1.0; reconstruction layer thickness: 2 mm. A total of three beds with 3 min per bed was collected for whole-body PET image acquisition. Tured system of post-processing workstation was used for image reconstruction to form transverse plane, coronal plane and sagittal plane and generate 3D projection image. Regions of interest (ROIs) on tumors or other research objects were manually outlined, and PET/CT workstation provided standardized uptake value (SUV) as the quantitative results. A nuclear medicine physician was responsible for identifying ROIs and measuring tumor SUV_{max} and tumor volume.

For ^{99m}Tc-HL-91 SPECT/CT, each model rabbit was injected with 7.4 MBq imaging agent. The scanning time points were set as 1.5 h P.I. A clinical SPECT/CT scanner (Symbia T16, Siemens, Germany) equipped with a low energy universal collimator was used. Rabbit models were anesthetized and scanned with the below parameters: energy peak: 141 keV; window width: ±10 %; matrix: 64 × 64; zoom: 1.45; time length of each slice: 30 s. CT image acquisition parameter was set as follows: tube voltage: 130 kV; tube current: 35 mA; and slice thickness: 2 mm. After acquisition was finished, coregistration of SPECT and CT images was performed. Volumes of interest (VOIs) were manually outlined on tumors and other research objects, and tracer uptake was defined as the percentage of injected dose per milliliter (%ID/mL).

For ¹⁸F-FDG PET/CT, the same scan parameters were set as ⁶⁸Ga-RGD PET/CT, but an item of F-18 was selected in the scanning system.

2.4. Evaluation of residual radioactivity and radiation exposure

In this research, the cumulative dosage of radiation was of the primary concern of the multiple NMIs. The radiation from residual radio-pharmaceutical was recorded via placing a radiation scanner (DT-9501, CEM-instruments, China) adjacent to the cage of injected rabbit. In addition, when fed in the cage, feces and urine were washed away with flowing water without delay. The measurement of cumulative dosage lasted for 24 h, specifically from the injection of ⁶⁸Ga-RGD to 24 h post the injection.

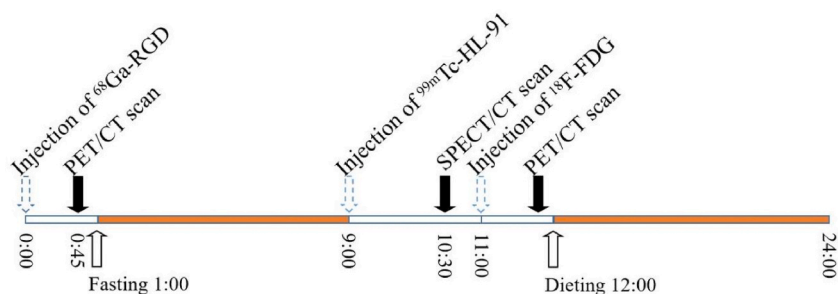


Fig. 1. Schematic diagram of one-day examination of triple nuclear medicine imaging, including the tracer injection, dieting plan, and schedules of ⁶⁸Ga-RGD PET/CT, ^{99m}Tc-HL-91 SPECT/CT and ¹⁸F-FDG PET/CT. The time lines in blank meant anaesthetic, and the ones in orange meant awake. (For interpretation of the references to colour in this figure legend, the reader is referred to the Web version of this article.)

2.5. Hemotoxylin and eosin staining and immunohistochemistry

Hemotoxylin and eosin (HE) staining and immunohistochemistry (IHC) analysis were performed on the tumorous tissues or interested tissues that were acquired at 12 h after the completion of triple nuclear medicine imaging. Vascular endothelial growth factor (VEGF) staining corresponded to ^{68}Ga -RGD PET/CT to detect the neovascularization in tissues surrounding to embolized lesion; Hypoxia-inducible factor 1 α (HIF-1 α) staining corresponded to $^{99\text{m}}\text{Tc}$ -HL-91 SPECT/CT to evaluate the anoxia of embolized lesion; and Ki-67 staining corresponded to ^{18}F -FDG PET/CT to evaluate the tumorous metabolism.

2.6. Statistics

The descriptive statistics, including PET/CT and SPECT/CT imaging, were computed on Prism software (Graphpad, La Jolla, CA, USA). All data analyses were performed using IBM SPSS Statistics software, version 20.0 (IBM Corporation, Armonk, NY, USA). If the data was in line with the normal distribution, *t*-test was utilized; otherwise, the nonparametric test analysis was utilized. Two-sided *P* values of less than 0.05 were considered to indicate statistically significant differences.

3. Results

Although the three radioactive tracers were separately injected with a minimum interval of 2 h, a longer period than the half-time in the serum, the stability in mixture was measured to confirm the feasibility of step-wise injection. Due to the distinct difference on the principle of nuclides-labeling, the excess unlabeled precursors did not affect the stability of accompanying radiopharmaceuticals, all of which maintained a radiochemical purity (RCP) of above 90 %. The typical TLC spectrum of ^{68}Ga -RGD, $^{99\text{m}}\text{Tc}$ -HL-91 and ^{18}F -FDG were provided in Fig. 2A, B and 2C, and the details of time-dependent stabilities were provided in Fig. 2D, E and 2F. A good stability of each radiopharmaceuticals in mixture was manifested.

Intraoperative and postoperative imaging of all three rabbit models showed good deposition of lipiodol in the VX2 tumor area of the left liver lobe, and the tumor contour was clearly visible (Fig. 3A). Lipiodol played a basic role of embolization, and tumor blood supply was completely or partially blocked (Fig. 3B). After the completion of embolization, the density of VX2 tumor area in each model was higher than that in other liver areas, and the lipiodol deposited in the tumor area showed nodular, mass, or ring deposition.

The radiation exposure of multiple nuclear medicine imaging was the first concern of clinical feasibility. Beside CT exposure, radiation exposure resulted from the radiopharmaceuticals during the scan and the following decay and metabolism was another main source. In this triple NMIs protocol, the radiation dosage from radiopharmaceuticals was limited below 5.70 ± 0.90 mSv. Take ^{68}Ga -RGD PET/CT as an example, the measured value of radiation was 2.55 ± 0.71 mSv at all. Fig. 4A drawn the theoretical value on the basis of physical decay and the corresponding measured value on the basis of physical decay together with biological metabolism, and Fig. 4B exhibited the accumulative tendency of radiation exposure. In addition, this protocol was consisted of three conventional CT scan, which can be replaced by MR imaging for a better radiation protection.

The multiple NMIs revealed the homogenesis and heterogenesis of prognosis post TAE. Although the suppressed glucose metabolism was detected in all (3/3) of the rabbit models in early response (9 days), the neovascularization was occasional in the local area around the tumor. The state of hypoxia was worsen post TAE in most tumorous tissues. Different with the suppressed tumor

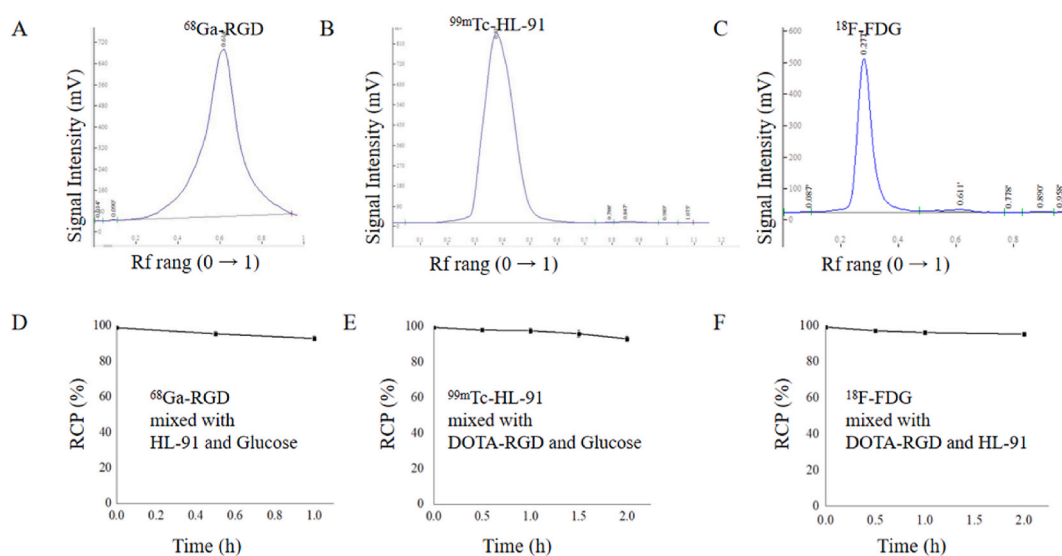


Fig. 2. The typical radio-TLC spectrum of ^{68}Ga -RGD (A), $^{99\text{m}}\text{Tc}$ -HL-91 (B) and ^{18}F -FDG (C), and the corresponding RCP of radiopharmaceutical co-incubated with precursors of the other ones.

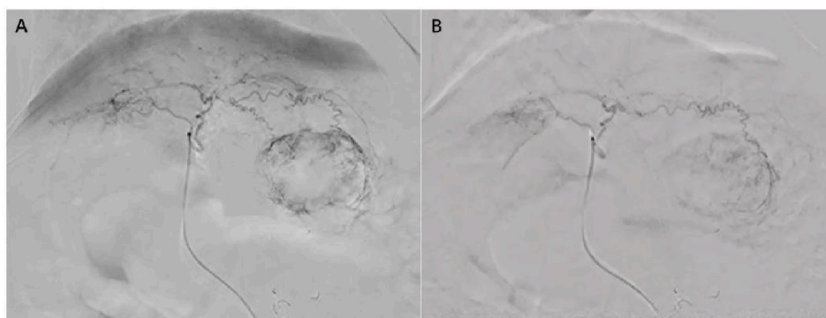


Fig. 3. Operation of transcatheterarterial embolization on rabbit model bearing VX2 tumor, including arterial angiogram of a rabbit liver (A) before embolization and near completion of embolization with lipiodol emulsion (B).

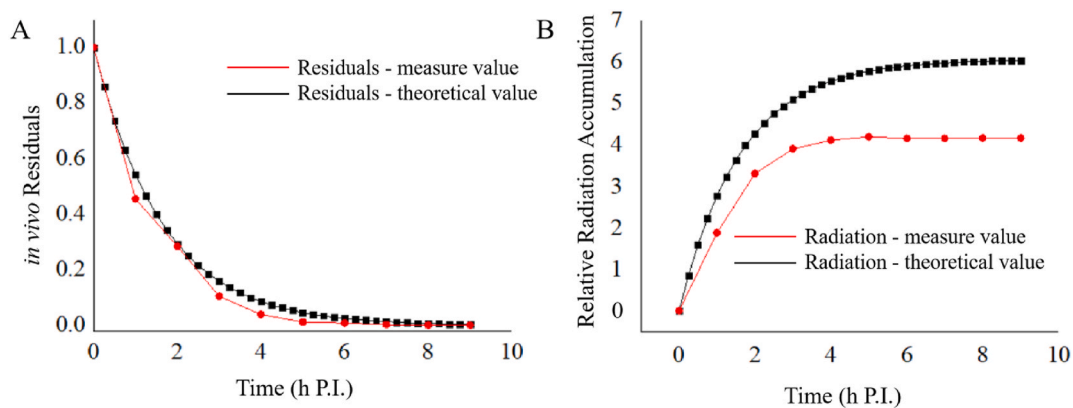


Fig. 4. The theoretical and measured radiation exposure of ^{68}Ga -RGD PET/CT. (A) the value of *in vivo* residuals, and (B) the accumulative tendency of radiation exposure.

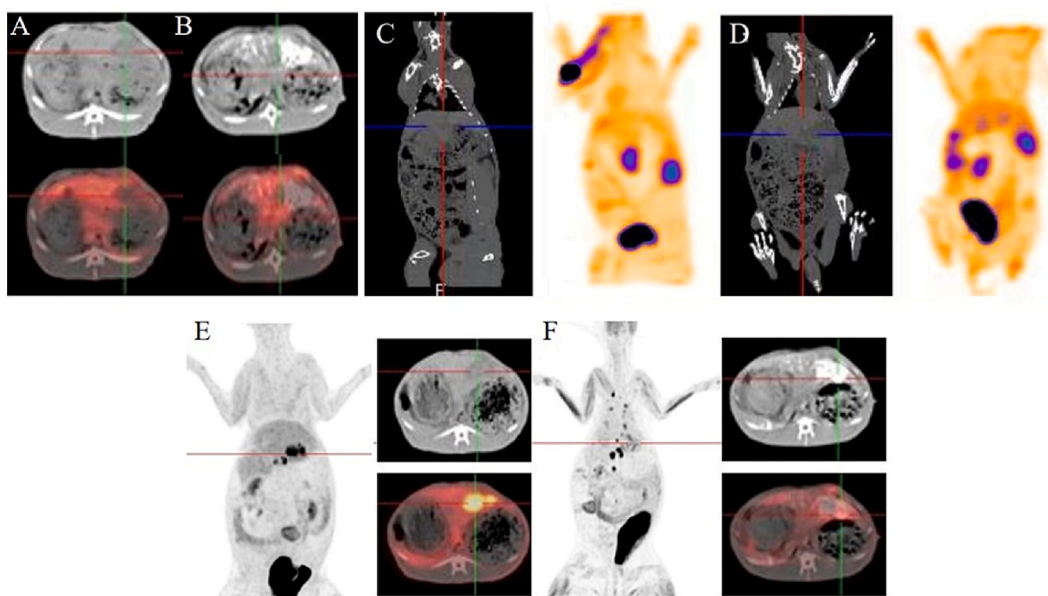


Fig. 5. One-day triple nuclear medicine imaging with ^{68}Ga -RGD PET/CT (A and B), $^{99\text{m}}\text{Tc}$ -HL-91 SPECT/CT (C and D) and ^{18}F -FDG PET/CT (E and F). The cross-line pointed to the lesions revealed by functional imaging.

metabolism, a diversity of pathological changes was revealed with multiple NMIs.

For example of the typical findings of rabbit models, the pre-operative ^{68}Ga -RGD PET/CT pictures (Fig. 5A) showed that there was slight to mild RGD uptake in the liver background of the rabbits ($\text{SUV}_{\text{max}} = 1.8$), and no significant RGD uptake was observed in the tumor area. One week after embolization, the post-operative imaging (Fig. 5B) showed the SUV_{max} of the normal liver parenchyma was slightly decreased, which is lower than the baseline value before embolization.

The coronal fusion image of HL-91 SPECT/CT showed the HL-91 uptake of the tumor and adjacent area before embolization were slight (Fig. 5C), while after embolization the uptake of HL-91 in the tumor and some adjacent areas was significantly higher than before (Fig. 5D). Lesional radioactivity intensity increased from $3551/\text{mm}^3$ to $7719/\text{mm}^3$. The ratio of radioactive counts in target to background region (muscle of left leg) was 5.830 after embolization, and that was 3.108 before embolization.

Baseline ^{18}F -FDG PET/CT (Fig. 5E) scan showed remarkable FDG accumulation in the tumor area ($\text{SUV}_{\text{max}} = 6.7$), and FDG uptake in nearby lymph nodes was also increased ($\text{SUV}_{\text{max}} = 6.5$). After embolization (Fig. 5F), the post-operative imaging (Figure E) revealed FDG uptake of tumor was significantly suppressed as no conspicuous uptake in most areas, and slight FDG uptake could be seen in a few residual areas ($\text{SUV}_{\text{max}} = 1.5$). Conversely, FDG uptake of nearby surrounding lymph nodes (no TAE treatment) were still obvious, and the SUV_{max} value was 7.9.

The result of HE and IHC analysis of tumors post TAE treatment were correspondingly shown in Fig. 6. A homogeneous nuclear staining was observed with Ki-67 (Fig. 6B). HIF-1 α immunoreactivity was nuclear and/or cytoplasmic (Fig. 6C), while it was perimembranous and/or diffuse cytoplasmic for VEGF (Fig. 6D). The arrows pointed to the positive staining in tumorous tissues. The HIF-1 α signaling was slightly positive and the expression of VEGF was obvious on the tissue.

The more important role of the multiple NMIs is detecting the heterogeneity of prognosis, for example of ^{18}F -FDG PET/CT (Fig. 7A), the VX2 tumor were ^{18}F -FDG-avid before treatment, the baseline SUV_{max} of VX2 tumor and the normal liver parenchyma was 6.75 and 1.83, respectively. The ratio of tumor to nontumor was 3.69. At 9 days post lipiodol TAE treatment, VX2 tumor uptake of ^{18}F -FDG was significantly decreased compared to the baseline value. The post-treatment tumor SUV_{max} was 3.25, and the tumor-to-nontumor ratio was 2.06.

In the case of ^{68}Ga -RGD PET/CT (Fig. 7B), the imaging revealed weak uptake in the primary lesion and rim of the tumor following lipiodol TAE treatment ($\text{SUV}_{\text{max}} = 0.69$), but there was mild ^{68}Ga -RGD uptake in the VX2 tumor prior to treatment ($\text{SUV}_{\text{max}} = 1.90$), which demonstrated the temporal suppression of neovasculature.

4. Discussion

^{18}F -FDG is an established broad spectrum tool for tumoral glucose metabolism. This approach may have applications for assessing residual tumor tissue or tumor progression [16]. As for liver cancer, the single ^{18}F -FDG imaging for diagnosing primary hepatocellular carcinoma (HCC) was not idealistic, especially for well-differentiated HCC. The cellular uptake of ^{18}F -FDG in HCC cells depends on the ratio of intracellular phosphokinase activity and glucose-6-phosphatase activity. The well-differentiated tumor cells are of higher concentrations of glucose-6-phosphatase and higher level of dephosphorylation, which accelerate the cell export process of ^{18}F -FDG

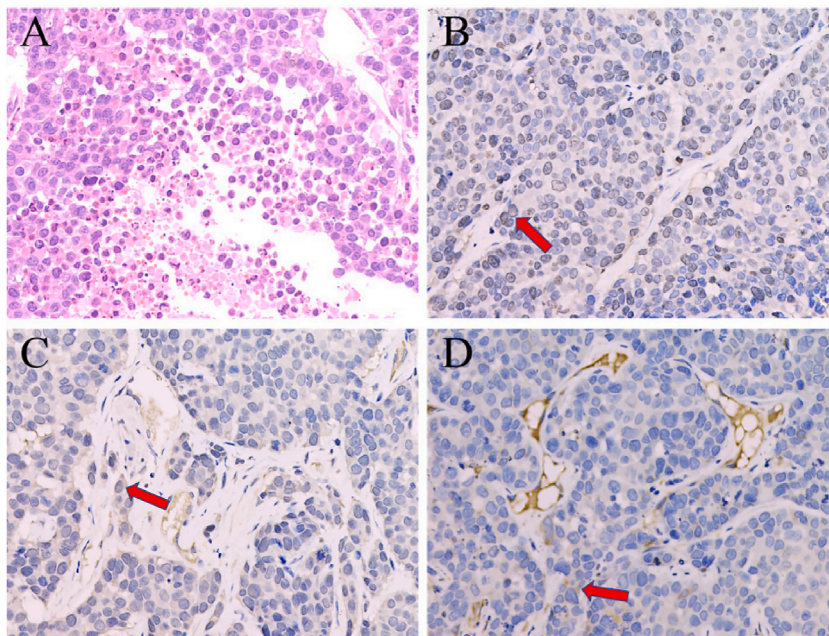


Fig. 6. HE staining (A) and IHC results of Ki-67 (B), HIF-1 α (C), and VEGF (D) in VX2 tumor tissue (magnification $\times 200$) that corresponded to NMIs in Fig. 5.

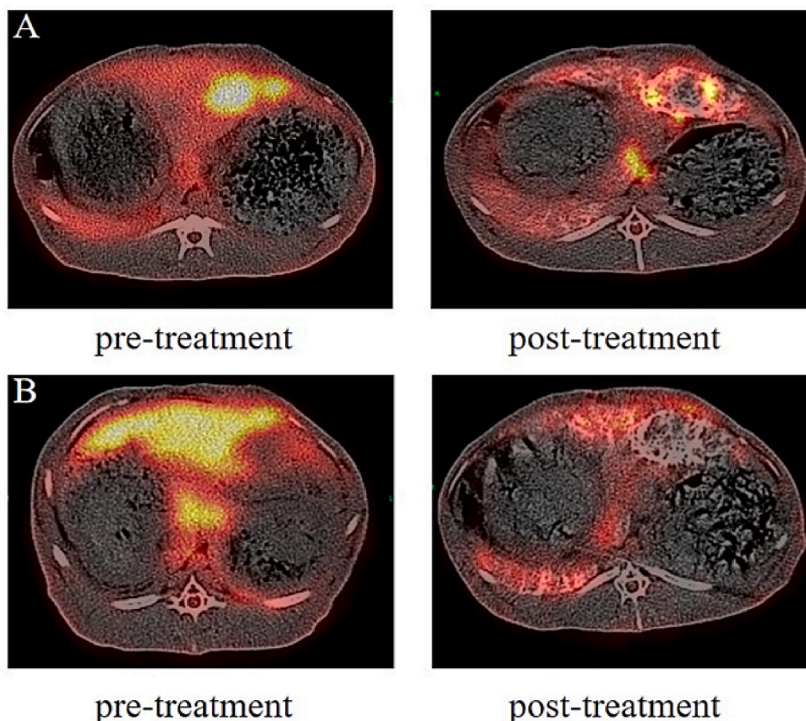


Fig. 7. Another example of double NMIs in evaluating TAE. (A) FDG PET manifested the suppressed tumor metabolic activity after embolization, and (B) RGD PET hinted the suppressed neovascularization post TAE.

[17]. In addition, pseudoprogression from immunotherapy can lead to increased tumor metabolic activity, so the "flare phenomenon" of FDG PET hinders the reliable identification of therapeutic effects [18]. As manifested in this research, comprehensive scans can increase confidence in assessing disease progression.

As performed in this research, TAE that based on lipiodol injection has sufficient clinical effectiveness for liver cancer [19], and has become the first-line treatment method for HCC in the intermediate stage. The tumoral environment after TAE is very complicated. The block of blood supply led by embolization will induce tissue hypoxia which result in cell damage and inhibit liver regeneration; besides, a major stimulus of angiogenesis and fibrogenesis and a promoter of liver carcinogenesis would also occur [20]. Tumor metabolism is always a prosperous research field, and the interrelation of tumor metabolism with hypoxia is complex [21]. Under hypoxic conditions, tumor cells can rapidly switch their glucose metabolism from oxidative to fermentative. Adaptation to low oxygen tension (hypoxia) in cells and tissues leads to the transcriptional induction of genes implicated in angiogenesis, erythropoiesis, glucose uptake and metabolism, cell proliferation, and survival. The main factor mediating this response is HIF-1 α , an oxygen-sensitive transcription factor [19], which induces VEGF expression and promotes neovascularization [22,23]. As shown in Figs. 5, Figs. 6 and 7, tumor heterogeneity existed in tumors treated with TAE, and was effectively manifested by the one-day examination of triple NMIs without delay to capture the varying tumor microenvironment. For instance, intrinsic structure defects of tumor neovascularization aggravate hypoxia, and start a vicious cycle of hypoxia and tumor neovascularization, inducing tumor recurrence and metastasis [24]. In addition to the one-day protocol already used, a variety of tumor-related molecular imaging methods can be incorporated into the combination of multiple NMIs. ^{11}C -acetate, as a precursor for amino acid and sterol synthesis, could significantly improve the sensitivity in diagnosing HCC [25].

In consideration of clinic developments, comprehensive treatment is an important direction of tumor therapy, which utilizes the complementarity of different treatment plans to improve the effectiveness. Except from the evaluation of tumor response, the triple nuclear imaging could also provide the reference for the comprehensive therapy of advanced HCC after the TACE or TARE. As a basic operation for efficient administration to the location of liver tumors, TAE has been proved to be synergistic with multiple treatment methods to further improve the efficacy of liver cancer, such as tyrosine kinase inhibitors (TKIs) therapy, immunotherapy, and radiotherapy [26,27]. For advanced HCC, the first-line recommended drug was tyrosine kinase inhibitors, but about 50 % patients are inherently resistant to sorafenib; moreover, acquired resistance appears for some patients during the medication process. Due to the difficulty in identifying the effective population before the therapy and observing acquired drug resistance, the prolongation of the median survival time in the overall population is only 2–3 months [28,29]. Therefore, liver cancer lacks effective targeted drugs, and lacks effective molecular markers or molecular typing based on the therapeutic effect of targeted drugs [28], and the detection of hypoxia and angiogenesis will provide the sufficient evidence for the drug decision. For TAE together with radiotherapy, tumor cells in a hypoxic environment are more radioresistant compared with the more radiosensitive oxygen-rich areas, resulting in a poorer

response to radiotherapy [30]. Not only for radiotherapy, the therapy on the basis of immune check point inhibitors, such as Nivolumab and Pembrolizumab, is influenced by the VEGF expression as well [31]. At this time, the expression of therapeutic biological targets or the expression of biologically characteristic molecules is of great value for the evaluation of comprehensive treatment effects, in this light, sub-classes of NMIs, such as immune PET and metabolic PET, are of great potentials [32]. All of the above methods can be superimposed with conventional FDG PET and other schemes to achieve a more comprehensive assessment of tumor metabolism and pathological changes based on molecular targeted imaging.

In a “real-world”, timeliness normally equals to a higher curative ratio, so the realization of one-day examination of multiple nuclear imaging is of clinical benefits for treatments planning, especially for those tumors in advanced stage. The information of radiation exposure is very meaningful to compare the risk/benefit for validation of NMI and contributes to optimizing protocol [33]. The published studies formally assessed whole-body dual-tracer PET/CT of ^{18}F -FDG and ^{11}C -acetate for HCC patients, which was of the maximum radiation-absorbed dose of about 29 mSv. If a contemporaneous contrast-enhanced abdomen CT was added, the effective dose was up to about 57 mSv [34]. In our study, this work mainly focused on the imaging of several nuclides with medium (physical) half-lives. The radiation exposure was controlled under 5.70 mSv for a model rabbit, manifesting the feasibility and bio-safety of one-day examination.

The choice of nuclides should cover the complementarity of ligand and radio-labeled chemistry. The advantage of this scheme is that the PET imaging agent with the longest half-life in the combination can be arranged as the last examination. Since there is no follow-up nuclear medicine examination, there will be no mutual interference between nuclear medicine signals. For the ECT examination used before the last PET examination, the characteristics of nuclides are fully considered, that is, most ECT nuclides will not produce detectable signals for PET scan (except for a few nuclides such as Y-90), because the energy of gamma photons is less than that of positrons. In fact, when selecting the nuclides with ultra-short half-lives, such as C-13, N-15 and O-17, the mutual influence of nuclide signals between different examinations can be further reduced.

As a preliminary research, some limitations were included in this research. First, the triple NMI was realized in modalities of both PET and SPECT, hence, the equipment of both PET and SPECT was necessary. When only PET equipped, double NMI with two PET scans was available. Secondly, the patients' willingness of triple injections will limit the application of triple NMI, and an informed consent with more details was essential.

5. Conclusions

Timely and integrated monitoring of oxygen level, tumor response of neovascularization, dynamic changes in glycolysis, and the evaluation of mutual relevance are very meaningful, especially for the individualized outcomes, and will contribute to making the reasonable treatment schedule, such as the timepoint of re-embolization. In this study, molecular probe $^{99\text{m}}\text{Tc}$ -HL91 SPECT reflecting the hypoxia situation, molecular probe ^{68}Ga -RGD PET targeting neovascularization and ^{18}F -FDG PET assessing tumor glycolysis, were integrated in one-day examination protocol. The triple nuclear imaging outlined a more comprehensive picture on pathological changes after TAE, that tumor metabolic activity was suppressed in 3/3 models, but localization and degree of hypoxia status and neovascularization varied individually, manifesting the necessity of integrated images analysis in dealing with complicated cases, which could not only facilitate testifying the validity of the one-day examination, but also possess the great clinical value.

Ethics statement

This research was approved by the Committee on Ethics of Medicine of Navy Medical University (No. 8220072600).

Funding statement

This work was funded by the National Natural Science Foundation of China (No. 81871390, 82302247), the Shanghai Pujiang Program (No. 2022PJD014).

CRedit authorship contribution statement

Nan Du: Conceptualization. **Guorong Jia:** Methodology. **Wen Zhang:** Methodology. **Qianqian Tong:** Validation. **Xudong Qu:** Formal analysis. **Danni Li:** Visualization. **Zhiping Yan:** Supervision. **Changjing Zuo:** Supervision. **Xiao Li:** Writing – original draft, Supervision, Conceptualization. **Rou Li:** Software, Investigation. **Wei Zhang:** Investigation.

Declaration of competing interest

The authors declare that they have no known competing financial interests or personal relationships that could have appeared to influence the work reported in this paper.

References

- [1] T. Jackson, C. Mosci, R. von Eyben, E. Mitra, K. Ganjoo, S. Biswal, S.S. Gambhir, A. Iagaru, Combined ^{18}F -NaF and ^{18}F -FDG PET/CT in the evaluation of sarcoma patients, *Clin. Nucl. Med.* 40 (9) (2015) 720–724, <https://doi.org/10.1097/RLU.0000000000000845>.

- [2] A. Iagaru, E. Mittra, S.S. Yaghoubi, D.W. Dick, A. Quon, M.L. Goris, S.S. Gambhir, Novel strategy for a cocktail ^{18}F -fluoride and ^{18}F -FDG PET/CT scan for evaluation of malignancy: results of the pilot-phase study, *J. Nucl. Med.* 50 (4) (2009) 501–505, <https://doi.org/10.2967/jnumed.108.058339>.
- [3] H. Kiat, G. Germano, J. Friedman, K. Van Train, G. Silagan, F.P. Wang, J. Maddahi, D. Berman, Comparative feasibility of separate or simultaneous rest thallium-201/stress technetium-99m-sestamibi dual-isotope myocardial perfusion SPECT, *J. Nucl. Med. Off. Publ. Soc. Nucl. Med.* 35 (4) (1994) 542–548.
- [4] A. Constantinesco, L. Mertz, B. Brunot, Myocardial perfusion and function imaging at rest with simultaneous thallium-201 and technetium-99m blood-pool dual-isotope gated SPECT, *J. Nucl. Med. Off. Publ. Soc. Nucl. Med.* 38 (3) (1997) 432–437.
- [5] J. Wang, T. Kondo, M. Tokuda, H. Shinozaki, M. Sarai, T. Yasui, J. Ishii, H. Kurokawa, M. Nomura, H. Hishida, Y. Watanabe, Vectorcardiographic evaluation of myocardial infarct size: comparisons with thallium myocardial scintigraphy, *Chin. Med. J. (Engl.)*. 112 (9) (1999) 780–786. PMID:11717944.
- [6] Y. Li, W. Zhang, H. Wu, G. Liu, Advanced tracers in PET imaging of cardiovascular disease, *BioMed Res. Int.* 2014 (2014) 1–13, <https://doi.org/10.1155/2014/504532>.
- [7] S.R. Katrin, V. Conrad-Amadeus, H. Lutz, W. Simone, S. Klaus, F. Thomas, M. Simone, E.D. Alexander, K. Carsten, Dual-tracer PET/CT protocol with [^{18}F]-FDG and [^{68}Ga]-Ga-FAPI-46 for cancer imaging - a proof of concept, *J. Nucl. Med.* 122 (2022) 263835, <https://doi.org/10.2967/jnumed.122.263835> jnumed.
- [8] P. Pessaux, V. Faucher, R. Cuny, M. Stephan, F. Klein, C. González, S. Blanes, E. Leost, B. Delattre, C. Lugiez, One-day diagnosis for hepatobiliary and pancreatic lesions: an innovative patient-centered care pathway organization, *J. Vis. Surg.* 155 (6) (2018) 439–443, <https://doi.org/10.1016/j.jvisurg.2018.02.005>.
- [9] C. Brogssitter, K. Zöphel, J. Kotzerke, ^{18}F -choline, ^{11}C -choline and ^{11}C -acetate PET/CT: comparative analysis for imaging prostate cancer patients, *Eur. J. Nucl. Med. Mol. Imag.* 40 (S1) (2013) 18–27, <https://doi.org/10.1007/s00259-013-2358-2>.
- [10] B.J. Beattie, P.M. Smith-Jones, Y.S. Jhanwar, H. Schöder, C.R. Schmidlein, M.J. Morris, P. Zanzonico, O. Squire, G.S.P. Meirelles, R. Finn, M. Namavari, S. Cai, H.I. Scher, S.M. Larson, J.L. Humm, Pharmacokinetic assessment of the uptake of 16β - ^{18}F -Fluoro-5 α -Dihydrotestosterone (FDHT) in prostate tumors as measured by PET, *J. Nucl. Med.* 51 (2) (2010) 183–192, <https://doi.org/10.2967/jnumed.109.066159>.
- [11] A. Santos, A. Mattioli, J.B. Carvalheira, U. Ferreira, M. Camacho, C. Silva, F. Costa, W. Matheus, M. Lima, E. Etchebehere, PSMA whole-body tumor burden in primary staging and biochemical recurrence of prostate cancer, *Eur. J. Nucl. Med. Mol. Imag.* 48 (2) (2021) 493–500, <https://doi.org/10.1007/s00259-020-04981-x>.
- [12] M.M. Queiroz, C.D.H. Lopes, A.C.R. Salgues, F. de G. Barbosa, E.S. Abe, T.P. Silveira, M.C.C. Machado, F.C. Capareli, ^{18}F -FDG PETCT and ^{68}Ga -DOTA PETCT mismatch with in vivo histopathological characterization of low-grade neuroendocrine pancreatic tumor, *Eur. J. Hybrid Imaging* 5 (1) (2021) 9, <https://doi.org/10.1186/s41824-021-00103-4>.
- [13] S. Gupta, A. Noor, H. Twigg, Hypoxic respiratory failure after transarterial embolization of hepatocellular carcinoma, *Chest* 142 (4) (2012) 1031A.
- [14] E.C. Ehman, M.S. Torbenson, C.L. Hallemeier, J.K. Heimbach, L.R. Roberts, Hepatocellular carcinoma, in: L.R. Roberts, J.D. Yang, S.K. Venkatesh (Eds.), *Evaluation and Management of Liver Masses*, Springer International Publishing, Cham, 2020, pp. 1–29.
- [15] T. Xue, W. Feng, H. Yu, M. Zhu, M. Fei, Y. Bao, X. Wang, W. Ma, G. Lv, J. Guan, S. Chen, Metastasis-associated protein 1 is involved in angiogenesis after transarterial chemoembolization treatment, *BioMed Res. Int.* 2017 (2017) 1–10, <https://doi.org/10.1155/2017/6757898>.
- [16] A. Leimgruber, K. Hickson, S.T. Lee, H.K. Gan, L.M. Cher, J.I. Sachinidis, G.J. O'Keefe, A.M. Scott, Spatial and quantitative mapping of glycolysis and hypoxia in glioblastoma as a predictor of radiotherapy response and sites of relapse, *Eur. J. Nucl. Med. Mol. Imag.* 47 (6) (2020) 1476–1485, <https://doi.org/10.1007/s00259-020-04706-0>.
- [17] K.T. Yoon, J.K. Kim, D.Y. Kim, S.H. Ahn, J.D. Lee, M. Yun, S.Y. Rha, C.Y. Chon, K.-H. Han, Role of ^{18}F -fluorodeoxyglucose positron emission tomography in detecting extrahepatic metastasis in pretreatment staging of hepatocellular carcinoma, *Oncology* 72 (Suppl. 1) (2007) 104–110, <https://doi.org/10.1159/00011715>.
- [18] T. Cascone, A. Weissferdt, M.C.B. Godoy, W.N. William, C.H. Leung, H.Y. Lin, S. Basu, S.S. Yadav, A. Pataer, K.G. Mitchell, M.A.W. Khan, Y. Shi, C. Haymaker, L. M. Solis, E.R. Parra, H. Kadara, I.I. Wistuba, P. Sharma, J.P. Allison, N.J. Ajami, J.A. Wargo, R.R. Jenq, D.L. Gibbons, J.J. Lee, S.G. Swisher, A.A. Vaporciyan, J. V. Heymach, B. Sepesi, Nodal immune flare mimics nodal disease progression following neoadjuvant immune checkpoint inhibitors in non-small cell lung cancer, *Nat. Commun.* 12 (1) (2021) 5045, <https://doi.org/10.1038/s41467-021-25188-0>.
- [19] P. Craig, S. Young, J. Golzarian, Current trends in the treatment of hepatocellular carcinoma with transarterial embolization: variability in technical aspects, *Cardiovasc. Intervent. Radiol.* 42 (9) (2019) 1322–1328, <https://doi.org/10.1007/s00270-019-02232-7>.
- [20] O. Rosmorduc, C. Housset, Hypoxia: a link between fibrogenesis, angiogenesis, and carcinogenesis in liver disease, *Semin. Liver Dis.* 30 (3) (2010) 258–270, <https://doi.org/10.1055/s-0030-1255355>.
- [21] A. Monteiro, R. Hill, G. Pilkington, P. Madureira, The role of hypoxia in glioblastoma invasion, *Cells* 6 (4) (2017) 45, <https://doi.org/10.3390/cells6040045>.
- [22] A. Sergio, C. Cristofori, R. Cardin, G. Pivetta, R. Ragazzi, A. Baldan, L. Girardi, U. Cillo, P. Burra, A. Giacomini, F. Farinati, Transcatheter arterial chemoembolization (TACE) in hepatocellular carcinoma (HCC): the role of angiogenesis and invasiveness, *Am. J. Gastroenterol.* 103 (4) (2008) 914–921, <https://doi.org/10.1111/j.1572-0241.2007.01712.x>.
- [23] X. Li, Expression of plasma vascular endothelial growth factor in patients with hepatocellular carcinoma and effect of transcatheter arterial chemoembolization therapy on plasma vascular endothelial growth factor level, *World J. Gastroenterol.* 10 (19) (2004) 2878, <https://doi.org/10.3748/wjg.v10.i19.2878>.
- [24] K. Liu, X.-L. Min, J. Peng, K. Yang, L. Yang, X.-M. Zhang, The changes of HIF-1 α and VEGF expression after TACE in patients with hepatocellular carcinoma, *J. Clin. Med. Res.* 8 (4) (2016) 297–302, <https://doi.org/10.14740/jocmr2496w>.
- [25] C.-L. Ho, S.C.H. Yu, D.W.C. Yeung, ^{11}C -acetate PET imaging in hepatocellular carcinoma and other liver masses, *J. Nucl. Med. Off. Publ. Soc. Nucl. Med.* 44 (2) (2003) 213–221. PMID: 12571212.
- [26] M. Tian, Y. Shi, W. Liu, J. Fan, Immunotherapy of hepatocellular carcinoma: strategies for combinatorial intervention, *Sci. China Life Sci.* 62 (9) (2019) 1138–1143, <https://doi.org/10.1007/s11427-018-9446-2>.
- [27] S. Shimose, T. Kawaguchi, H. Iwamoto, T. Niizeki, T. Shirono, M. Tanaka, H. Koga, T. Torimura, Indication of suitable transarterial chemoembolization and multikinase inhibitors for intermediate stage hepatocellular carcinoma, *Oncol. Lett.* 19 (4) (2020) 2667–2676, <https://doi.org/10.3892/ol.2020.11399>.
- [28] J.M. Llovet, V. Hernandez-Gea, Hepatocellular carcinoma: reasons for phase III failure and novel perspectives on trial design, *Clin. Cancer Res.* 20 (8) (2014) 2072–2079, <https://doi.org/10.1158/1078-0432.CCR-13-0547>.
- [29] A.-L. Cheng, Y.-K. Kang, Z. Chen, C.-J. Tsao, S. Qin, J.S. Kim, R. Luo, J. Feng, S. Ye, T.-S. Yang, J. Xu, Y. Sun, H. Liang, J. Liu, J. Wang, W.Y. Tak, H. Pan, K. Burock, J. Zou, D. Voliotis, Z. Guan, Efficacy and safety of sorafenib in patients in the asia-pacific region with advanced hepatocellular carcinoma: a phase III randomised, double-blind, placebo-controlled trial, *Lancet Oncol.* 10 (1) (2009) 25–34, [https://doi.org/10.1016/S1470-2045\(08\)70285-7](https://doi.org/10.1016/S1470-2045(08)70285-7).
- [30] J.N. Rich, Cancer stem cells in radiation resistance, *Cancer Res.* 67 (19) (2007) 8980–8984, <https://doi.org/10.1158/0008-5472.CAN-07-0895>.
- [31] X. Liu, Y. Lu, S. Qin, Atezolizumab and bevacizumab for hepatocellular carcinoma: mechanism, pharmacokinetics and future treatment strategies, *Future Oncol.* 17 (17) (2021) 2243–2256, <https://doi.org/10.2217/fon-2020-1290>.
- [32] W. Wei, Z.T. Rosenkrans, J. Liu, G. Huang, Q.-Y. Luo, W. Cai, ImmunoPET: concept, design, and applications, *Chem. Rev.* 120 (8) (2020) 3787–3851, <https://doi.org/10.1021/acs.chemrev.9b00738>.
- [33] R.J. Pentreath, Radiological protection and the exposure of animals as patients in veterinary medicine, *J. Radiol. Prot.* 36 (2) (2016) N42–N45, <https://doi.org/10.1088/0952-4746/36/2/N42>.
- [34] D. Liu, P.-L. Khong, Y. Gao, U. Mahmood, B. Quinn, J. St Germain, X.G. Xu, L.T. Dauer, Radiation dosimetry of whole-body dual-tracer ^{18}F -FDG and ^{11}C -acetate PET/CT for hepatocellular carcinoma, *J. Nucl. Med.* 57 (6) (2016) 907–912, <https://doi.org/10.2967/jnumed.115.165944>.